Supplementary Material

Abstract

This document is the supplementary material for the article "Reconfigurable Massive MIMO: Harnessing the Power of the Electromagnetic Domain for Enhanced Information Transfer". Three parts of the original article are presented in a more detailed form. The first part is the channel modeling of reconfigurable massive MIMO (R-mMIMO) systems. The second part is the pseudo-code of the proposed EMR domain precoding algorithm. The final part gives a detailed description of the modeling in Fig. 1 of the article.

I. Channel Model for R-mMIMO systems

We consider a general point-to-point R-mMIMO system with N_r receive antennas and N_t transmit antennas. The channel model in our article can be derived by making some simplifications to the general model. We assume that the n_t-th transmit antenna utilizes the μ_{n_t}-th radiation pattern and the n_r-th receive antenna utilizes the ν_{n_r}-th radiation pattern, respectively. Here, $\mu_{n_t} \in \mathcal{S}_t$, and $\mathcal{S}_t \triangleq \{\bar{\mu}_0, \bar{\mu}_1, \cdots, \bar{\mu}_{P_t-1}\}$ is the set of available antenna radiation patterns for the RPA at the transmitter. Similarly, $\nu_{n_r} \in \mathcal{S}_r$, and $\mathcal{S}_r \triangleq \{\bar{\nu}_0, \bar{\nu}_1, \cdots, \bar{\nu}_{P_r-1}\}$ is the set of available antenna radiation patterns for the RPA at the receiver. By referring to [1], the time-delay (t, τ) domain channel between the n_t-th transmit antenna and the n_r-th receive antenna is denoted by $H_{n_r,n_t}(t, \tau; \nu_{n_r}, \mu_{n_t})$, which is given by

$$\begin{aligned} H_{n_r,n_t}(t,\tau;\nu_{n_r},\mu_{n_t}) = \sum_{l=1}^{L} \alpha_l \boldsymbol{f}^{\mathrm{T}}_{\mathrm{rx},n_r}(\theta_{r,l},\phi_{r,l};\nu_{n_r}) \boldsymbol{T}_l \boldsymbol{f}_{\mathrm{tx},n_t}(\theta_{t,l},\phi_{t,l};\mu_{n_t}) \exp\left(\frac{\mathrm{j}2\pi\left(\boldsymbol{r}^{\mathrm{T}}_{\mathrm{rx},l}\boldsymbol{d}_{\mathrm{rx},n_r}\right)}{\lambda}\right) \\ \times \exp\left(\frac{\mathrm{j}2\pi\left(\boldsymbol{r}^{\mathrm{T}}_{\mathrm{tx},l}\boldsymbol{d}_{\mathrm{tx},n_t}\right)}{\lambda}\right) \exp\left(\frac{\mathrm{j}2\pi\left(\boldsymbol{r}^{\mathrm{T}}_{\mathrm{rx},l}\boldsymbol{v}\right)}{\lambda} t\right) \delta\left(\tau - \tau_l\right), \end{aligned} \tag{1}$$

where the definition of each variable is given in Table I. Furthermore, by restricting the user

TABLE I: Channel model for R-mMIMO systems

Parameter	Definition	Parameter	Definition
α_l	Channel gain for l-th path	λ	Wavelength
L	Total number of paths	τ_l	Channel delay for l-th path
$\boldsymbol{T}_l \in \mathbb{C}^{2\times 2}$	Polarization coupling matrix for l-th path	$\boldsymbol{v} \in \mathbb{R}^3$	UE velocity vector
$(\theta_{r.l}, \phi_{r,l})$	Elevation/azimuth angle for l-th arrival path	$(\theta_{t,l}, \phi_{t,l})$	Elevation/azimuth angle for l-th departure path
$\boldsymbol{f}_{\mathrm{rx},n_r}(\theta_{r,l}, \phi_{r,l}; \nu_{n_r}) \in \mathbb{R}^2$	Radiation pattern of n_r-th receive antenna	$\boldsymbol{f}_{\mathrm{tx},n_t}(\theta_{t,l}, \phi_{t,l}; \mu_{n_t}) \in \mathbb{R}^2$	Radiation pattern of n_t-th transmit antenna
$\boldsymbol{r}_{\mathrm{rx},l} \in \mathbb{R}^3$	Spherical unit vector for l-th arrival path	$\boldsymbol{r}_{\mathrm{tx},l} \in \mathbb{R}^3$	Spherical unit vector for l-th departure path
$\boldsymbol{d}_{\mathrm{rx},n_r} \in \mathbb{R}^3$	Location vector of n_r-th receive antenna	$\boldsymbol{d}_{\mathrm{tx},n_t} \in \mathbb{R}^3$	Location vector of n_t-th transmit antenna
B_w	System bandwidth	K	Total number of subcarriers

equipment (UE) to deploy a single non-reconfigurable antenna, as the article assumes, we can derive the degraded channel model between each UE and the BS as follows

$$\begin{aligned} h_{n_t}(t,\tau;\mu_{n_t}) = \sum_{l=1}^{L} \alpha_l \boldsymbol{f}_{\mathrm{rx}}^{\mathrm{T}}(\theta_{r,l},\phi_{r,l}) \boldsymbol{T}_l \boldsymbol{f}_{\mathrm{tx},n_t}(\theta_{t,l},\phi_{t,l};\mu_{n_t}) \exp\left(\frac{\mathrm{j}2\pi\left(\boldsymbol{r}_{\mathrm{rx},l}^{\mathrm{T}}\boldsymbol{d}_{\mathrm{rx}}\right)}{\lambda}\right) \\ \times \exp\left(\frac{\mathrm{j}2\pi\left(\boldsymbol{r}_{\mathrm{tx},l}^{\mathrm{T}}\boldsymbol{d}_{\mathrm{tx},n_t}\right)}{\lambda}\right) \exp\left(\frac{\mathrm{j}2\pi\left(\boldsymbol{r}_{\mathrm{rx},l}^{\mathrm{T}}\boldsymbol{v}\right)}{\lambda} t\right) \delta\left(\tau-\tau_l\right). \end{aligned} \tag{2}$$

Then, after transforming the time-delay (t,τ) domain channel to the time-frequency (t,k) domain channel, the channel between each UE and the n_t-th antenna of the BS can be rewritten as follows

$$\begin{aligned} h_{n_t}(t,k;\mu_{n_t}) = \sum_{l=1}^{L} \alpha_l \boldsymbol{f}_{\mathrm{rx}}^{\mathrm{T}}(\theta_{r,l},\phi_{r,l}) \boldsymbol{T}_l \boldsymbol{f}_{\mathrm{tx},n_t}(\theta_{t,l},\phi_{t,l};\mu_{n_t}) \exp\left(\frac{\mathrm{j}2\pi\left(\boldsymbol{r}_{\mathrm{rx},l}^{\mathrm{T}}\boldsymbol{d}_{\mathrm{rx}}\right)}{\lambda}\right) \\ \times \exp\left(\frac{\mathrm{j}2\pi\left(\boldsymbol{r}_{\mathrm{tx},l}^{\mathrm{T}}\boldsymbol{d}_{\mathrm{tx},n_t}\right)}{\lambda}\right) \exp\left(\frac{\mathrm{j}2\pi\left(\boldsymbol{r}_{\mathrm{rx},l}^{\mathrm{T}}\boldsymbol{v}\right)}{\lambda} t\right) \exp\left(\mathrm{j}2\pi\tau_l\left(-\frac{B_w}{2}+\frac{B_w k}{K}\right)\right). \end{aligned} \tag{3}$$

Particularly, for the sake of notational simplicity in the article, we drop the time index t and frequency index k, and use $\boldsymbol{h}_u(\boldsymbol{\mu})$ to represent the channel vector between the u-th UE and the BS instead, i.e., $[\boldsymbol{h}_u(\boldsymbol{\mu})]_{n_t} = h_{n_t}(t,k;\mu_{n_t})$. Such simplification is based on the fact that the radiation pattern only has an impact on the channel gain. This can be explained as follows.

As shown in Equ. (2), the radiation pattern terms $\boldsymbol{f}_{\mathrm{tx},n_t}(\theta_{t,l},\phi_{t,l};\mu_{n_t}) \in \mathbb{R}^2$ and $\boldsymbol{f}_{\mathrm{rx},n_r}(\theta_{r,l},\phi_{r,l};\nu_{n_r}) \in \mathbb{R}^2$ make the R-mMIMO system different from conventional MIMO systems. In conventional MIMO systems, the modeling of the radiation pattern is usually neglected (i.e., an ideal omnidirectional antenna is assumed and the signals coming from every direction have the same gains when sampled by the radiation pattern). Such simplification is reasonable for system analysis, however, the inherent electromagnetic (EM) properties are overlooked.

Specifically, the radiation pattern is an EM level property of an antenna, where the information of both the radiation pattern shape and the polarization direction is contained. Let us explain the polarization first. As shown in Equ. (2), the two components of $\boldsymbol{f}_{\mathrm{tx},n_t}(\theta_{t,l},\phi_{t,l};\mu_{n_t})$ correspond to two orthogonal polarization directions. If a vertical-polarized EM wave is received by a horizontal-polarized antenna, then no signal can be detected. For practical complex environments, the polarization coupling matrix $\boldsymbol{T}_l \in \mathbb{C}^{2\times 2}$ is used to model the transformation of polarization direction when the transmitted signal is affected by diffraction, reflection, and scattering. The effects of $\boldsymbol{f}^{\mathrm{T}}_{\mathrm{rx},n_r}(\theta_{r,l},\phi_{r,l};\nu_{n_r})\boldsymbol{T}_l\boldsymbol{f}_{\mathrm{tx},n_t}(\theta_{t,l},\phi_{t,l};\mu_{n_t})$ are finally combined into a scalar which influences the channel gain. Rather than changing the polarization property of the antenna, our article only considers the reconfigurability of the shape of the radiation pattern with the assistance of the parasitic layer. Its influence on the channel can also be captured by a change of the channel gains. However, the adjustment to the radiation pattern affects all the multipath components simultaneously. Under such circumstances, the RPA can redistribute the relative path gain among multipath components. With this extra degree of freedom (DoF) in the EM radiation domain, more favorable channel conditions can be customized according to the specific optimization target.

II. EMR DOMAIN PRECODING ALGORITHM

The **EMR domain precoding algorithm** in the original article only gives a literal description, a more rigorous pseudo-code description of this algorithm is given below. The spectral efficiency (SE) is calculated as Equ. (4). Here, u and k are indexes for UE and subcarrier, respectively. $\boldsymbol{F}_{RF} \in \mathbb{C}^{N_t\times M_t}$ is the analog precoder, and $\boldsymbol{f}_{u,k} \in \mathbb{C}^{M_t}$ is the digital precoder. Besides, the n_t-th element of $\boldsymbol{h}_u^{\mathrm{H}}(t,k;\boldsymbol{\mu})$ is generated by $h(t,k;\mu_{n_t})$.

$$R=\frac{1}{K}\sum_{u=1}^{U}\sum_{k=1}^{K}\log\left(1+\frac{|\boldsymbol{h}_u^{\mathrm{H}}(t,k;\boldsymbol{\mu})\,\boldsymbol{F}_{\mathrm{RF}}\boldsymbol{f}_{u,k}|^2}{\sum\limits_{j\neq u}^{U}|\boldsymbol{h}_u^{H}(t,k;\boldsymbol{\mu})\,\boldsymbol{F}_{\mathrm{RF}}\boldsymbol{f}_{j,k}|^2+\sigma_n^2}\right), \tag{4}$$

III. MODELING OF FIG. 1

In Fig. I, we consider the electric(E)-field generated by a uniform linear array (ULA) at a fixed point $P(0,y_0,z_0)$. We assume a ULA with $2N+1$ array elements is placed along the z-axis with its geometric center at the origin, as illustrated in Fig. II. Without loss of

Algorithm 1: EMR domain precoding algorithm

Input: CSI $\boldsymbol{h}_{u,k}\left(\boldsymbol{\mu}\right), \forall u, k, \boldsymbol{\mu}$;

Output: EMR domain precoding vector $\boldsymbol{\mu}^{\star}$;

Initialization: $\boldsymbol{\mu}^{0} = \mathbf{0}_{N_t}$;

for $i = 1 : T_{iter}$ **do**

  for $n_t = 1 : N_t$ **do**

    for $p = 0 : P-1$ **do**

      $\widetilde{\boldsymbol{\mu}} = \left\{\mu_l = \mu_l^i, l < n_t, \mu_{n_t} = \bar{\mu}_p, \qquad \mu_m = \mu_m^{i-1}, m > n_t\right\}$;

      Apply HP to CSI $\boldsymbol{h}_{u,k}\left(\widetilde{\boldsymbol{\mu}}\right), \forall u, k$, and calculate SE value $R_p = R\left(\boldsymbol{h}_{u,k}\left(\widetilde{\boldsymbol{\mu}}\right), \forall u, k\right)$ according to Equ. (2);

    end

    $p^{\star} = \arg \max_{0 \le p \le P-1} R_p$;

    $\mu_{n_t}^i = \bar{\mu}_{p^{\star}}$;

  end

end

return $\boldsymbol{\mu}^{\star} = \boldsymbol{\mu}^{T_{iter}}$.

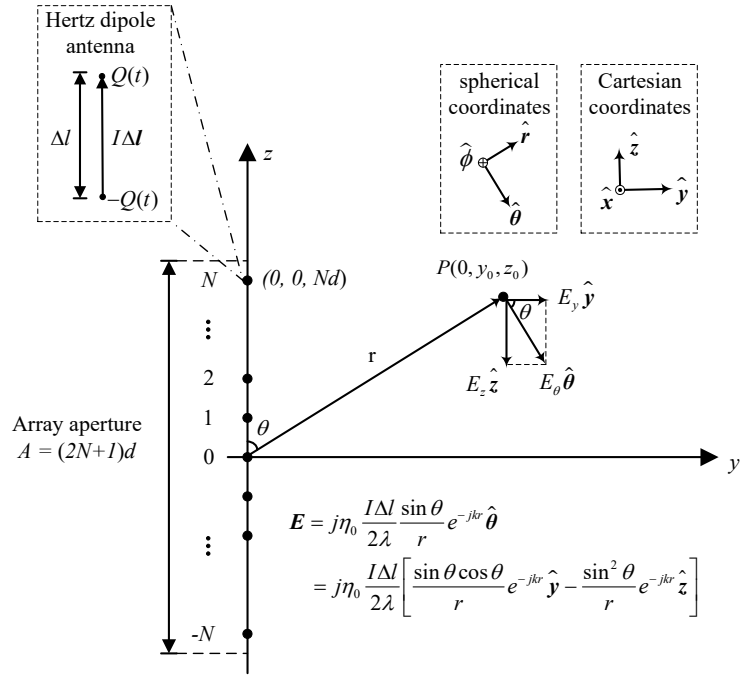

Fig. I. Illustrative model of Fig. 1 in the article.

generality, each antenna element of the ULA is modeled as a Hertz dipole antenna (HPA) for its tractable EM radiation expression. We assume a fully-digital architecture is adopted for this ULA array, which means the radiation of each antenna element can be independently controlled by the corresponding input excitation current. To explain the differences between T-mMIMO, R-mMIMO, and HMIMO in our context, we first detail the radiation E-field from a single HPA in free space.

The E-field expression of an HPA (far-field approximation) in spherical coordinates can be obtained from Maxwells' equations as follows [3] .

$$\boldsymbol{E} = E_\theta \hat{\boldsymbol{\theta}} = j\eta_0 \frac{I_0 \Delta l}{2\lambda} \frac{e^{-jkr}}{r} \sin\theta \hat{\boldsymbol{\theta}}, \tag{5}$$

where $\eta_0 = 120\pi\,(\Omega)$ is the free-space impedance, I_0 is the current intensity flowing through the HPA, λ is the operation wavelength, $k = 2\pi/\lambda$ is the wavenumber, $\Delta l < \lambda$ is the length (size) of the HPA, $r = \sqrt{y_0^2 + (z_0 - z')^2}$ is the distance between the source $O(0, 0, z')$ and the target point $P(0, y_0, z_0)$, $\sin\theta = \frac{y_0}{r}$ is the sine of zenith angle θ, and $\hat{\boldsymbol{\theta}}$ is the unit spherical basis vector corresponding to the zenith angle. Besides, we also define $\hat{\boldsymbol{\phi}}$ as the spherical basis vector corresponding to the azimuth angle, as illustrated in Fig. II. Note that the HPA has no E-field component in $\hat{\boldsymbol{\phi}}$ direction. Then, the radiation pattern of an HPA, defined as the E-field intensity normalized by its maximum value, is given by

$$F(\theta) = \frac{|E_\theta|}{\max(|E_\theta|)} = \sin\theta. \tag{6}$$

Now, we introduce R-mMIMO to this specific example. Following the basic idea of the reconfigurable antenna in our article, we assume the radiation direction of each HPA's pattern can be changed through electric tuning methods. This borrows the idea of the ESPAR antenna [2] (a type of antenna whose radiation direction can be electrically rotated in the plane through a change of the reactive loading). By fixing the HPA's position but changing the flow direction of the current on it, the far-field E-field of this reconfigurable HPA can be expressed as

$$\boldsymbol{E}' = E'_\theta \hat{\boldsymbol{\theta}} = j\eta_0 \frac{I_0 \Delta l}{2\lambda} \frac{e^{-jkr}}{r} \sin(\theta - \theta_0)\, \hat{\boldsymbol{\theta}}, \tag{7}$$

where θ_0 is a tunable parameter that decides the maximum radiation direction. In this case, the radiation pattern of such reconfigurable HPA is given by $F'(\theta; \theta_0) = \sin(\theta - \theta_0)$. Note that such R-mMIMO assumption does not conflict with the parasitic layer-based architecture in Section III, since they both follow the same idea of having adjustable radiation patterns, and the system

assumed for Fig. 1 is only a toy model to simplify the analysis. Based on Equ. (5) and Equ. (7), we explain the differences among T-mMIMO, R-mMIMO, and HMIMO in the following:

- **T-mMIMO**: Each antenna is modeled by an HPA, whose radiation pattern is fixed, i.e., Equ. (5), and the whole array is composed of a massive number of discrete antenna elements;
- **R-mMIMO**: Each antenna is modeled by a reconfigurable HPA, whose radiation pattern is tunable, i.e., Equ. (7), and the whole array is composed of a massive number of discrete antenna elements;
- **HMIMO**: Each antenna is modeled by a reconfigurable HPA, whose radiation pattern is tunable, i.e., Equ. (7). By fixing the array aperture, we reduce the antenna spacing when increasing the number of array elements, the HMIMO is obtained as the number of antenna elements goes to infinity.

For the T-mMIMO array, the E-field intensity at point P is the superposition of each HPA's radiation E-field, and it is given by

$$\boldsymbol{E}_r = \frac{j\eta_0 \Delta l}{2\lambda}\left(\sum_{n=-N}^{N} I_{0,n}\frac{\sin\theta_n\cos\theta_n}{r_n}e^{-j\frac{2\pi}{\lambda}r_n}\hat{\boldsymbol{y}} - \sum_{n=-N}^{N} I_{0,n}\frac{\sin^2\theta_n}{r_n}e^{-j\frac{2\pi}{\lambda}r_n}\hat{\boldsymbol{z}}\right). \tag{8}$$

Here, we have changed the spherical coordinates into Cartesian coordinates for ease of vector superposition. $I_{0,n}$ is the excitation current intensity at the n-th antenna, and r_n, $\sin\theta_n$, and $\cos\theta_n$ are respectively given by

$$r_n = \sqrt{y_0^2 + (z_0 - nd)^2}, \tag{9a}$$

$$\sin\theta_n = \frac{y_0}{r_n} = \frac{y_0}{\sqrt{y_0^2 + (z_0 - nd)^2}}, \tag{9b}$$

$$\cos\theta_n = \frac{z_0 - nd}{r_n} = \frac{z_0 - nd}{\sqrt{y_0^2 + (z_0 - nd)^2}}, \tag{9c}$$

where d is the distance between two adjacent antenna elements. To maximize the received energy at $P(0, y_0, z_0)$, we need to design the excitation current $\{I_{0,n}\}_{n=-N}^{N}$ so that the received E-intensity $\boldsymbol{E}_r$ is maximized. This design target leads to the following optimization problem

$$\begin{aligned} \min_{\{I_{0,n}\}_{n=-N}^{N}} \quad & |\boldsymbol{E}_r|^2, \\ \text{s.t.} \quad & \textstyle\sum_{n=-N}^{N} |I_{0,n}|^2 \Delta l \leq P_t. \end{aligned} \tag{10}$$

Here, $|\boldsymbol{E}_r|^2 = |\sum_{n=-N}^{N} \frac{j\eta_0 I_{0,n}\Delta l}{2\lambda}\frac{\sin\theta_n\cos\theta_n}{r_n}e^{-j\frac{2\pi}{\lambda}r_n}|^2 + |\sum_{n=-N}^{N} -\frac{j\eta_0 I_{0,n}\Delta l}{2\lambda}\frac{\sin^2\theta_n}{r_n}e^{-j\frac{2\pi}{\lambda}r_n}|^2$ is the superimposed E-field intensity, P_t is the total power constraint. For notational simplicity, let $\boldsymbol{w} =$

$[I_{0,-N},\cdots,I_{0,N}]^T \in \mathbb{C}^{2N+1}$ denotes the current vector to be optimized. Besides, by defining $\boldsymbol{e}_y = \left[\frac{j\eta_0\Delta l}{2\lambda}\frac{\sin\theta_{-N}\cos\theta_{-N}}{r_{-N}}e^{-j\frac{2\pi}{\lambda}r_{-N}},\cdots,\frac{j\eta_0 I_{0,n}\Delta l}{2\lambda}\frac{\sin\theta_n\cos\theta_n}{r_n}e^{-j\frac{2\pi}{\lambda}r_n},\cdots,\frac{j\eta_0 I_{0,n}\Delta l}{2\lambda}\frac{\sin\theta_N\cos\theta_N}{r_N}e^{-j\frac{2\pi}{\lambda}r_N}\right]^T$, $\boldsymbol{e}_z = \left[-\frac{j\eta_0\Delta l}{2\lambda}\frac{\sin^2\theta_{-N}}{r_{-N}}e^{-j\frac{2\pi}{\lambda}r_{-N}},\cdots,-\frac{j\eta_0\Delta l}{2\lambda}\frac{\sin^2\theta_n}{r_n}e^{-j\frac{2\pi}{\lambda}r_n},\cdots,-\frac{j\eta_0\Delta l}{2\lambda}\frac{\sin^2\theta_N}{r_N}e^{-j\frac{2\pi}{\lambda}r_N}\right]^T$, the above optimization problem is rewritten as

$$\begin{aligned}\min_{\boldsymbol{w}} \quad & \boldsymbol{w}^H(\boldsymbol{e}_y\boldsymbol{e}_y^H+\boldsymbol{e}_z\boldsymbol{e}_z^H)\boldsymbol{w},\\ \text{s.t.} \quad & \boldsymbol{w}\boldsymbol{w}^H\Delta l\leq P_t.\end{aligned} \tag{11}$$

This is a typical Rayleigh quotient maximization problem, whose optimal solution is given by the maximum eigenvector of the matrix $\boldsymbol{T}=\boldsymbol{e}_y\boldsymbol{e}_y^H+\boldsymbol{e}_z\boldsymbol{e}_z^H$. Denoting the maximum eigenvalue of $\boldsymbol{T}$ by λ_1 and the corresponding eigenvector by $\boldsymbol{u_1}$, then the optimal $\boldsymbol{w}^*$ and the corresponding objective value are given by

$$\boldsymbol{w}^* = \sqrt{\frac{P_t}{\Delta l}}\boldsymbol{u}_1, \tag{12a}$$

$$(|\boldsymbol{E}_r|^2)^* = \frac{P_t}{\Delta l}\lambda_1. \tag{12b}$$

Now, we have derived the maximum E-field intensity for T-mMIMO at any target point $P(0,y_0,z_0)$. We further derive the received E-intensity for R-mMIMO. Similar to T-mMIMO, the major difference between T-mMIMO and R-mMIMO lies in the radiation pattern. The superimposed E-field generated by R-mMIMO at point $P(0,y_0,z_0)$ is given by

$$\boldsymbol{E}_r' = \frac{j\eta_0\Delta l}{2\lambda}\left(\sum_{n=-N}^{N} I_{0,n}\frac{\sin(\theta_n-\theta_{0,n})\cos\theta_n}{r_n}e^{-j\frac{2\pi}{\lambda}r_n}\hat{\boldsymbol{y}} - \sum_{n=-N}^{N} I_{0,n}\frac{\sin(\theta_n-\theta_{0,n})\sin\theta_n}{r_n}e^{-j\frac{2\pi}{\lambda}r_n}\hat{\boldsymbol{z}}\right), \tag{13}$$

where $\theta_{0,n}$ is the central radiation direction of the n-th reconfigurable antenna. Different from T-mMIMO where we can only optimize $\{I_{0,n}\}_{n=-N}^N$, we can optimize both $\{\theta_{0,n}\}_{n=-N}^N$ and $\{I_{0,n}\}_{n=-N}^N$ for R-mMIMO. Note that when the target point P is located in the far-field region, the maximum angle of view between P and the array is an acute angle (this can be verified with the simulation parameters below), which means the largest angle spanned by all the E-field vectors generated by reconfigurable antennas is also an acute angle. According to the property of the superposition of the vectors, to maximize the modulus of $\boldsymbol{E_r}$, the modulus of each component needs to be maximized. It is obvious that $\theta_n-\theta_{0,n}=\frac{\pi}{2},\forall n$, can produce the maximum modulus, and the E-field intensity is further simplified as

$$\boldsymbol{E}_r' = \frac{j\eta_0\Delta l}{2\lambda}\left(\sum_{n=-N}^{N} I_{0,n}\frac{\cos\theta_n}{r_n}e^{-j\frac{2\pi}{\lambda}r_n}\hat{\boldsymbol{y}} - \sum_{n=-N}^{N} I_{0,n}\frac{\sin\theta_n}{r_n}e^{-j\frac{2\pi}{\lambda}r_n}\hat{\boldsymbol{z}}\right), \tag{14}$$

Similar to T-mMIMO, we respectively define $\boldsymbol{w}$, $\boldsymbol{e}_y$, and $\boldsymbol{e}_z$ as $\boldsymbol{w} = [I_{0,-N}, \cdots, I_{0,N}]^T \in \mathbb{C}^{2N+1}$, $\boldsymbol{e}_y = \left[\frac{j\eta_0\Delta l}{2\lambda}\frac{\cos\theta_n}{r_{-N}}e^{-j\frac{2\pi}{\lambda}r_{-N}}, \cdots, \frac{j\eta_0\Delta l}{2\lambda}\frac{\cos\theta_n}{r_n}e^{-j\frac{2\pi}{\lambda}r_n}, \cdots, \frac{j\eta_0\Delta l}{2\lambda}\frac{\cos\theta_n}{r_N}e^{-j\frac{2\pi}{\lambda}r_N}\right]^T \in \mathbb{C}^{2N+1}$, and $\boldsymbol{e}_z = \left[-\frac{j\eta_0\Delta l}{2\lambda}\frac{\sin\theta_n}{r_{-N}}e^{-j\frac{2\pi}{\lambda}r_{-N}}, \cdots, -\frac{j\eta_0\Delta l}{2\lambda}\frac{\sin\theta_n}{r_n}e^{-j\frac{2\pi}{\lambda}r_n}, \cdots, -\frac{j\eta_0\Delta l}{2\lambda}\frac{\sin\theta_n}{r_N}e^{-j\frac{2\pi}{\lambda}r_N}\right]^T \in \mathbb{C}^{2N+1}$. Similar to T-mMIMO, $\boldsymbol{T} = \boldsymbol{e}_y\boldsymbol{e}_y^H + \boldsymbol{e}_z\boldsymbol{e}_z^H$ in the objective function is a rank-2 matrix. The optimal solution to this E-intensity maximum problem can be efficiently solved by eigenvalue decomposition (EVD).

For a finite number of antenna elements, the maximum E-intensity at target point $P(0, y_0, z_0)$ can be solved through the above EVD method. However, we are also interested in the HMIMO case when the number of antenna elements goes to infinity. A closed-form expression for the E-intensity is desired for computational simplicity. In this case, we assume that the antenna aperture A is fixed, and we change the antenna spacing d when increasing the number of antennas N, which leads to

$$(2N+1)d = A. \tag{15}$$

Starting with $\boldsymbol{T} = \boldsymbol{e}_y\boldsymbol{e}_y^H + \boldsymbol{e}_z\boldsymbol{e}_z^H$, we hope to find the asymptotic maximum value of $(|\boldsymbol{E}_r'|^2)^*$ as N goes to infinity. To evaluate the performance of HMIMO, we first introduce the following Proposition.

Proposition 1. For an arbitrary rank-2 matrix $\boldsymbol{T} = \boldsymbol{e}_y\boldsymbol{e}_y^H + \boldsymbol{e}_z\boldsymbol{e}_z^H$, with $\boldsymbol{e}_y^H\boldsymbol{e}_y \neq 0$, the largest eigenvalue of $\boldsymbol{T}$ is given by

$$\lambda_1 = \max\{t_1b_0 + c_0, t_2b_0 + c_0\} = \frac{(a_0 + c_0) + \sqrt{(a_0 - c_0)^2 + 4b_0^2}}{2}, \tag{16}$$

where t_1, t_2 are the solutions to the equation $b_0t^2 + (c_0 - a_0)t - b_0^* = 0$, where

$$\begin{gathered} a_0 = (1 + |m|^2)||\boldsymbol{e}_y||_2^2, \quad b_0 = -m^*||\boldsymbol{e}_y||_2||\tilde{\boldsymbol{e}}_z||_2, \quad c_0 = ||\tilde{\boldsymbol{e}}_z||_2^2, \\ m = -\frac{\boldsymbol{e}_y^H\boldsymbol{e}_z}{\boldsymbol{e}_y^H\boldsymbol{e}_y}, \quad \tilde{\boldsymbol{e}}_z = \boldsymbol{e}_z + m\boldsymbol{e}_y. \end{gathered} \tag{17}$$

The corresponding eigenvector is given by $\boldsymbol{u}_1 = \tilde{k}(t_1\frac{\boldsymbol{e}_y}{||\boldsymbol{e}_y||_2} + \frac{\tilde{\boldsymbol{e}}_z}{||\tilde{\boldsymbol{e}}_z||_2})$. Here, $\tilde{k}$ is the normalization coefficient which makes $\boldsymbol{u}_1$ have unit power.

Proof. See Appendix A.

According to Equ. (12b), the maximum E-field intensity of at point $P(0, y_0, z_0)$ is given by $(|\boldsymbol{E}_r'|^2)^* = \frac{P_t}{\Delta l}\lambda_1$. To obtain $\lim\limits_{N\to\infty}|\boldsymbol{E}_r'|^2 = P_t\lim\limits_{N\to\infty}\frac{\lambda_1}{\Delta l}$, we have to determine the following limits first

$$\lim_{N\to\infty}\frac{\boldsymbol{e}_y^H\boldsymbol{e}_z}{\Delta l} = \lim_{N\to\infty}\sum_n(-\tilde{E}_0^2)\frac{\sin\theta_n\cos\theta_n}{r_n^2}\Delta l = (-\tilde{E}_0^2)\lim_{N\to\infty}\sum_n\frac{y_0\,(z_0 - nd)}{\left[y_0^2 + (z_0 - nd)^2\right]^2}\Delta l, \tag{18a}$$

$$\lim_{N\to\infty}\frac{\boldsymbol{e}_y^H\boldsymbol{e}_y}{\Delta l}=\lim_{N\to\infty}\sum_n\tilde{E}_0^2\frac{\cos^2\theta_n}{r_n^2}\Delta l=\tilde{E}_0^2\lim_{N\to\infty}\sum_n\frac{(z_0-nd)^2}{\left[y_0^2+(z_0-nd)^2\right]^2}\Delta l, \tag{18b}$$

$$\lim_{N\to\infty}\frac{\boldsymbol{e}_z^H\boldsymbol{e}_z}{\Delta l}=\lim_{N\to\infty}\sum_n\tilde{E}_0^2\frac{\sin^2\theta_n}{r_n^2}\Delta l=\tilde{E}_0^2\lim_{N\to\infty}\sum_n\frac{y_0^2}{\left[y_0^2+(z_0-nd)^2\right]^2}\Delta l, \tag{18c}$$

where $\tilde{E}_0=\frac{\eta_0}{2\lambda}$ is a constant. The above limits can be approximated by integrals when $\lim_{N\to\infty}d=\lim_{N\to\infty}\frac{A}{2N+1}=0$. In this case, the length of each array element also has to be infinitesimal, i.e., $\lim_{N\to\infty}\Delta l=dl$. Then the asymptotic value of Equ. (18) can be calculated from the following integrals:

$$\lim_{N\to\infty}\frac{\boldsymbol{e}_y^H\boldsymbol{e}_z}{\Delta}=-\tilde{E_0}^2\int_{-A/2}^{A/2}\frac{y_0(z_0-l)}{[y_0^2+(z_0-l)^2]^2}dl=\frac{\tilde{E_0}^2}{y_0}\left(-\frac{\cos 2\alpha}{4}\Big|_{\alpha_1}^{\alpha_2}\right), \tag{19a}$$

$$\lim_{N\to\infty}\frac{\boldsymbol{e}_y^H\boldsymbol{e}_y}{\Delta}=\tilde{E_0}^2\int_{-A/2}^{A/2}\frac{(z_0-l)^2}{[y_0^2+(z_0-l)^2]^2}dl=-\frac{\tilde{E_0}^2}{y_0}\left(\frac{1}{2}\alpha-\frac{1}{4}\sin 2\alpha\Big|_{\alpha_1}^{\alpha_2}\right), \tag{19b}$$

$$\lim_{N\to\infty}\frac{\boldsymbol{e}_z^H\boldsymbol{e}_z}{\Delta}=\tilde{E_0}^2\int_{-A/2}^{A/2}\frac{y_0^2}{[y_0^2+(z_0-l)^2]^2}dl=-\frac{\tilde{E_0}^2}{y_0}\left(\frac{1}{2}\alpha+\frac{1}{4}\sin 2\alpha\Big|_{\alpha_1}^{\alpha_2}\right), \tag{19c}$$

where $\alpha_2=\tan^{-1}(\frac{z_0-A/2}{y_0}),\ \alpha_1=\tan^{-1}(\frac{z_0+A/2}{y_0})$. By substituting Equ. (19) into Equ. (16), (17), we obtain the performance limit of HMIMO and the corresponding weight $\boldsymbol{w}^*$.

So far, we have provided the method for calculating the maximum received E-intensity at point $P(0,y_0,z_0)$ for T-mMIMO, R-mMIMO, and HMIMO, respectively. To show the statistical difference of the maximum E-intensity among different MIMO architectures, we randomly generated point P in the region of $\{(0,y,z)\,|\,y\in[5,50]\,m, z\in[50,100]\,m\}$. By averaging the results over $3,000$ Monte Carlo simulations, we obtained Fig. 1 in the article. In addition, the antenna aperture and the carrier frequency were set as $A=4\lambda$ and $f_c=3$ GHz, respectively.

APPENDIX A
PROOF OF PROPOSITION 1

Proposition 1 aims at finding the maximum eigenvalue and corresponding eigenvector of a rank-2 matrix $\boldsymbol{A}=\boldsymbol{x}\boldsymbol{x}^H+\boldsymbol{y}\boldsymbol{y}^H$, where $\boldsymbol{x}$ and $\boldsymbol{y}$ are both non-zero vectors of the same length. To begin with, we construct two orthogonal vectors which span the space of matrix $\boldsymbol{A}$ as follows

$$\tilde{\boldsymbol{x}}=\boldsymbol{x}, \tag{20a}$$

$$\tilde{\boldsymbol{y}}=\boldsymbol{y}+m\boldsymbol{x}, \tag{20b}$$

where $m = -\frac{\boldsymbol{x}^H \boldsymbol{y}}{\boldsymbol{x}^H \boldsymbol{x}}$ is a scalar coefficient guaranteeing the orthogonality $\tilde{\boldsymbol{x}}^H \tilde{\boldsymbol{y}} = 0$. Then, the normalized vectors $\boldsymbol{u}_1 = \frac{\boldsymbol{x}}{\|\boldsymbol{x}\|_2}$ and $\boldsymbol{u}_2 = \frac{\tilde{\boldsymbol{y}}}{\|\tilde{\boldsymbol{y}}\|_2}$ constitute two eigenvectors of $\boldsymbol{A}$. Then, we need to find the eigenvalue which satisfies the following equation:

$$\boldsymbol{A}\left(k_1 \boldsymbol{u}_1 + k_2 \boldsymbol{u}_2\right) = \lambda \left(k_1 \boldsymbol{u}_1 + k_2 \boldsymbol{u}_2\right). \tag{21}$$

By substituting the expressions for $\boldsymbol{u}_1$ and $\boldsymbol{u}_2$ in the left side of (21), we obtain

$$\boldsymbol{A}\boldsymbol{u}_1 = \left(1 + |m|^2\right) \|\boldsymbol{x}\|_2^2 \frac{\boldsymbol{x}}{\|\boldsymbol{x}\|_2} - m^* \|\boldsymbol{x}\|_2 \|\tilde{\boldsymbol{y}}\|_2 \frac{\tilde{\boldsymbol{y}}}{\|\tilde{\boldsymbol{y}}\|_2}, \tag{22a}$$

$$\boldsymbol{A}\boldsymbol{u}_2 = -m \|\boldsymbol{x}\|_2 \|\tilde{\boldsymbol{y}}\|_2 \frac{\boldsymbol{x}}{\|\boldsymbol{x}\|_2} + \|\tilde{\boldsymbol{y}}\|_2^2 \frac{\tilde{\boldsymbol{y}}}{\|\tilde{\boldsymbol{y}}\|_2}. \tag{22b}$$

By further defining $a_0 = (1 + |m|^2) \|\boldsymbol{x}\|_2^2$, $b_0 = -m^* \|\boldsymbol{x}\|_2 \|\tilde{\boldsymbol{y}}\|_2$, and $c_0 = \|\tilde{\boldsymbol{y}}\|_2^2$, the left side of (21) is further simplified as follows,

$$\boldsymbol{A}\left(k_1 \boldsymbol{u}_1 + k_2 \boldsymbol{u}_2\right) = \left(k_1 a_0 + k_2 b_0^*\right) \boldsymbol{u}_1 + \left(k_1 b_0 + k_2 c_0\right) \boldsymbol{u}_2. \tag{23}$$

By comparing (23) with the right side of (21), we have

$$\lambda = \frac{k_1 a_0 + k_2 b_0^*}{k_1} = \frac{k_1 b_0 + k_2 c_0}{k_2}. \tag{24}$$

Since k_1 and k_2 are non-zero, we define $t = \frac{k_1}{k_2}$, then (24) is transformed to the following equation

$$b_0 t^2 + (c_0 - a_0) t - b_0^* = 0. \tag{25}$$

It is obvious that the maximum eigenvalue can be obtained as $\lambda_m = \max\{t_1 b_0 + c_0, t_2 b_0 + c_0\}$, and the corresponding eigenvector is $\boldsymbol{u}_m = \tilde{k}(t_m \frac{\boldsymbol{x}}{||\boldsymbol{x}||_2} + \frac{\tilde{\boldsymbol{y}}}{||\tilde{\boldsymbol{y}}||_2})$. Here, $\tilde{k}$ is the normalization coefficient, which ensures that $\boldsymbol{u}_1$ has unit power, and t_m is the solution of (25) corresponding to λ_m.

REFERENCES

[1] 3GPP, "Study on channel model for frequencies from 0.5 to 100 GHz," 3rd Generation Partnership Project (3GPP), Technical Report (TR) 38.901, 05 2017, version 14.0.0.

[2] R. Harrington, "Reactively controlled directive arrays," *Trans. Antennas Propag.*, vol. 26, no. 3, pp. 390-395, May 1978.

[3] D. Cheng, *Field and wave electromagnetics*, 2nd, Addison-Wesley, 1989.